



# Soil–Water Retention Curve Prediction for Compacted London Clay Subjected to Moisture Cycles

Ana Sofia Dias · Paul N. Hughes ·  
David G. Toll

Received: 5 June 2023 / Accepted: 5 November 2023 / Published online: 23 November 2023  
© The Author(s) 2023

**Abstract** The evolution of the hydraulic properties of London Clay when compacted at a range of initial conditions (density and water content) was investigated. The soil–water retention curve (SWRC) is observed to change as the soil is subjected to cycles of wetting and drying. A new method is presented for predicting these changes in the soil–water retention curves (SWRCs) based on the starting conditions for each cycle. The method is based on relationships between the degree of saturation before drying ( $S_{r,i}$ ), which includes the effect of void ratio and soil fabric, and key parameters that characterize the shape of SWRCs (air-entry value and slope of the transition zone). The relationship between the  $S_{r,i}$  and the air-entry value (or yield point, YP), and the relationship between the YP and the slope of the transition zone of the SWRC were established for the large experimental data set of two types of London clay of high and very high plasticity. The fitting parameters of a bi-linear SWRC model were estimated and used to constrain the fitting parameters of the van Genuchten model. As the SWRC of compacted clay continuously

changes with progressive moisture cycles, this model allows the prediction of this evolution for the modelling of earthworks over the years, when subject to changing climatic conditions, without the need for an extensive experimental program.

**Keywords** Unsaturated soils · Soil–water retention curve · Compacted soil · High plasticity clay

## 1 Introduction

The Soil Water Retention Curve (SWRC) represents the relationship between water content (or degree of saturation) and suction and is a key property in understanding unsaturated soil behaviour (Fredlund 2000). Azizi et al. (2020) and Stirling et al. (2021), among others, demonstrated that a key aspect of the deterioration process of soil in infrastructure embankments (e.g. for railways and roads) is that cycles of drying and wetting produce changes in the soil–water retention behaviour. Therefore, quantifying the evolution of the soil–water retention behaviour of clay soils is essential to understand the mechanism of deterioration (loss of strength with time) of compacted clay fill materials subject to seasonal moisture cycles. This understanding is exceptionally important for managing ageing earthworks supporting the transport infrastructure in the UK under more extreme climatic conditions (Clarke and Smethurst 2010; Muddle et al. 2015; Ferranti et al. 2018; Walker et al.

---

A. S. Dias (✉) · P. N. Hughes · D. G. Toll  
Department of Engineering, Durham University, Durham,  
UK  
e-mail: ana.s.dias@durham.ac.uk

P. N. Hughes  
e-mail: paul.hughes2@durham.ac.uk

D. G. Toll  
e-mail: d.g.toll@durham.ac.uk

2022). London Clay, which is present along the transport infrastructure mostly in Southern England (UK), has so far been less investigated. Dias et al. (2023a) showed that the SWRC and the shrink-swell behaviour of compacted London clay presented irreversible changes for different intensities of suction during drying–wetting cycles, in which greater changes were observed after extending the drying phase.

Cycles of wetting and drying have been observed to produce changes in SWRCs through the progressive decrease of the AEV, reduction of the hysteresis and progressively lower suctions for the same water content (Lin and Cerato 2013; Seiphoori et al. 2014; Stirling et al. 2017; Azizi et al. 2020; Liu et al. 2020; Ng and Peprah-Manu 2023), which consequently result in lower soil strength. Similarly, studies on volumetric deformations caused by moisture cycles attribute the progressive evolution of soil shrinkage curves to rearrangement of soil particles, which will in turn affect the SWRC. The accumulation of deformations with cycling shows that soil does not present a fully elastic behaviour and it is described as fatigue (Dif and Bluemel 1991; Tripathy and Subba Rao 2009; Estabragh et al. 2015). Nonetheless, some of the limitations of previous studies lie in: (i) not measuring volume changes (Jayanth et al. 2012; Zeng et al. 2019; Wen et al. 2020); (ii) performing limited number of cycles (Lin and Cerato 2013; Seiphoori et al. 2014; Al Haj and Standing 2016; Stirling et al. 2017) while other studies demonstrated that a greater number of moisture cycles is required to attain a stable state (Dif and Bluemel 1991; Tripathy and Subba Rao 2009; Estabragh et al. 2015); and (iii) no previous studies that systematically investigate different initial compaction conditions (i.e., compaction water content and density state).

It has been shown that the shape of the SWRC is influenced by the compaction conditions, i.e. the void ratio and water content (Romero et al. 1999, 2011; Villar 2007; Birlle et al. 2008). Studies have related these key parameters characterizing the SWRC shape to different soil properties, such as a relationship between the void ratio at compaction and the air-entry value (AEV), a relationship between the AEV and the slope of the SWRC (Karube and Kawai 2001; Salager et al. 2010; Kawai et al. 2020), and relationships between soil physical properties and the SWRC shape (Romero and Vaunat 2000; Wang et al. 2020). However, very few studies have investigated which

factors play a role in the evolution of the SWRC with drying–wetting cycles. So far, it has been observed that the SWRCs of loose silt require more moisture cycles to reach equilibrium (Ng and Peprah-Manu 2023), and dense clay presented cumulative swelling, while loose clay presented shrinkage behaviour with cycling (Nowamooz and Masrouri 2010). Rearrangement of soil particles and changes in the micro-structure observed in the pore-size distribution have been identified as the source of such changes in the SWRC (Seiphoori et al. 2014; Sun et al. 2019).

In the present study, an experimental programme was carried out to produce a unique and comprehensive data set, by testing two sources of London Clay (high and very high plasticity according to the classification of the BS1377; BSI 1990), each compacted at five different water contents and void ratio states, and where samples from each starting condition were subjected to up to 16 cycles of drying and wetting; many more than has been investigated in previous studies. This data allows us to further the understanding of how different compaction conditions, varying water content and void ratio, influence the evolution of the SWRC of London Clay. An empirical model is here presented that allows the changes in the SWRC with moisture cycles to be predicted. The model is based on the evolution of the parameters observed over the first six drying–wetting cycles and is then used to predict the final stages of drying and wetting. The combination of multiple soil types, large range of starting conditions and high number of wetting–drying cycles tested within this study has enabled a more comprehensive analysis of the complex changes to SWRCs induced by wetting–drying cycles than has previously been possible.

## 2 Experimental Methods and Materials

### 2.1 Soil Characterization

London Clay from two different locations were used for testing: high plasticity (HP) clay was obtained from Clapham; and very high plasticity (VHP) clay was collected from Vauxhall, both in London (UK). A detailed characterization of the tested clays is presented in Table 1. The characterization tests, and resultant classifications, were conducted in accordance with BS1377 (BSI 1990). The tested clay

**Table 1** Properties of the tested clays (high plasticity, HP; and very high plasticity, VHP) (Dias et al. 2023b)

Plasticity classification BS1377 (BSI 1990)	High plasticity (HP)	Very high plasticity (VHP)
Location	Clapham	Vauxhall
Specific gravity	2.77	2.78
Clay (%)	41	54
Silt (%)	49	42
Sand (%)	10	4
Liquid limit (%)	60	77
Plasticity index (%)	36	53
Clay activity	0.88	0.98
Proctor optimum water content (%)	22	22
Proctor maximum dry density (Mg m <sup>-3</sup> )	1.58	1.59

presented normal activity as it took values above 0.75 and below 1.25, similarly to typical values reported for London Clay of 0.95 (Skempton 1984).

### 2.2 Sample Preparation

The optimum water content obtained from Proctor compaction tests was 0.22 (22%) for both clays. The maximum dry density was 1.58 Mg m<sup>-3</sup> (void ratio of e=0.75) for the high plasticity clay and 1.59 Mg m<sup>-3</sup> (e=0.75) for the very high plasticity clay (Table 1). The samples were compacted at five different conditions, varying the water content (w) or the dry density relative to the Proctor optimum as shown in Table 2. The representation on the compaction plane with the respective compaction curve is presented in Fig. 1.

Specimens identified as ‘loose’ and ‘dense’ were prepared at the same water content as the ‘optimum’ state (w=0.21 to 0.22) but using different levels of compaction stress to achieve looser or denser states. Specimens identified as ‘wet’ and ‘dry’ were prepared at wetter (w=0.24) and dryer conditions (w=0.20) but compacted to achieve approximately the same density as the ‘optimum’ state (e=0.77 and 0.76). Part of the tests here presented have been reported in Dias et al. (2023b).

To prepare the soil for testing, the air-dried clay was passed through a sieve with an opening of 2 mm. The passing fraction was mixed with distilled water to obtain the chosen water contents for compaction. Static compaction was used to prepare samples with a diameter of 15 mm and a height of 5 mm. The

**Table 2** Compacted conditions of samples of each clay (high plasticity, HP; and very high plasticity, VHP): void ratio (e), gravimetric water content (w), degree of saturation (S<sub>r</sub>), and

total suction (s); and the total number of drying–wetting cycles performed (Dias et al. 2023b)

Clay	State of compaction	Void ratio (e)	Gravimetric water content (w)	Degree of saturation (S <sub>r</sub> )	Total suction (s) (MPa)	No. of cycles
HP	Loose	0.95	0.22	0.63	1.75	13
HP	Optimum	0.77	0.22	0.78	1.58	14
HP	Dense	0.64	0.22	0.94	1.78	11
HP	Wet	0.77	0.24	0.85	1.53	13
HP	Dry	0.75	0.20	0.74	1.22	13
VHP	Loose	0.95	0.21	0.62	1.11	13
VHP	Optimum	0.76	0.21	0.77	1.50	13
VHP	Dense	0.62	0.21	0.94	1.51	16
VHP	Wet	0.77	0.24	0.85	1.21	13
VHP	Dry	0.79	0.20	0.69	2.28	13

properties of each sample are shown in Table 2. The void ratio at compaction varied between 0.62 and 0.95, the initial water content varied between 0.20 and 0.24, and the initial total suction (measured using a WP4C dewpoint potentiometer) varied between 1.11 and 2.28 MPa.

### 2.3 Measurement of the Soil–Water Retention Curves

The soil–water retention curves (SWRCs) were determined by measuring the degree of saturation (determined from gravimetric water content and void ratio) and total suction. The gravimetric water content was determined from weight variations of samples measured using a balance with a precision of 0.0001 g. Total suction was measured by a chilled mirror dew point potentiometer (Decagon Devices WP4C).

The volume changes were determined by measuring the height and diameter of the samples using a digital caliper (accuracy of 0.01 mm). A similar method has been used in previous studies, such as Cornelis et al. (2006), Leong and Wijaya (2015), Al Haj and Standing (2016), and Mishra et al. (2020), among others. Other methods of measuring volume changes are: displacement methods (not appropriate for the present study due to its destructive nature); 3D scanning (expensive and time consuming); and Digital Image Correlation (requires the samples to be stationary) (Leong and Wijaya 2015). Therefore, direct measurement using a caliper was identified to be the best suited for the present study. There can be errors in the measurement if the samples become irregular shaped, but it was observed that the geometry of the soil samples was maintained throughout the testing. The diameter and height of the samples was measured three times to estimate the volume based on the average value, minimizing the error. The changes in samples included the formation of cracks, hence these are considered in the estimated degree of saturation.

Six cycles of drying and wetting were imposed onto the samples between 1 and 80 MPa, providing an insight into the behaviour of compacted London Clay in the range of suctions controlled by the intra-aggregate water exchanges (Romero and Vauvat 2000). This range covers the expected AEV of this soil, the region of the SWRC which presents the greatest variation of water content with suction,

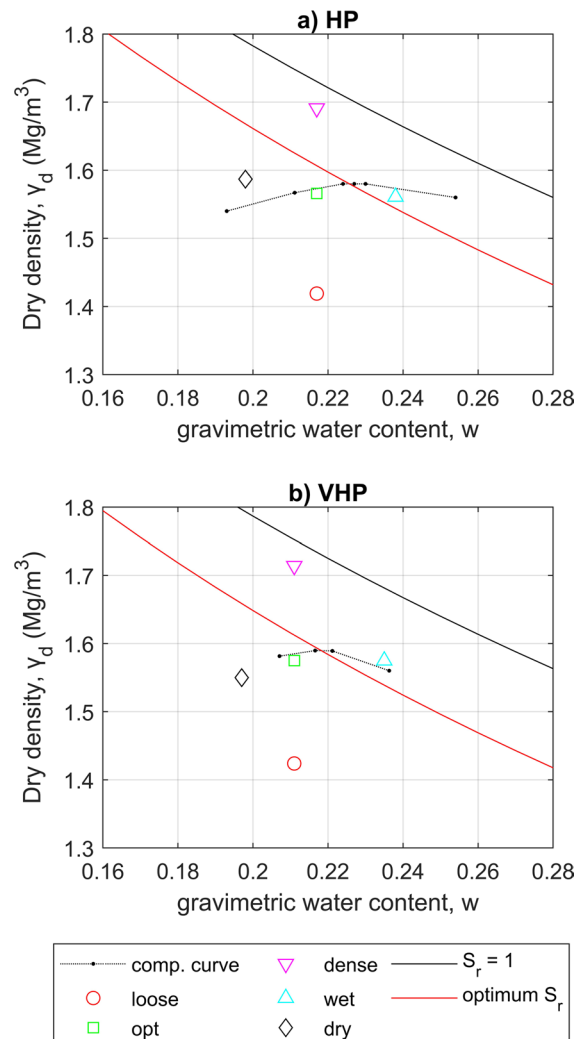
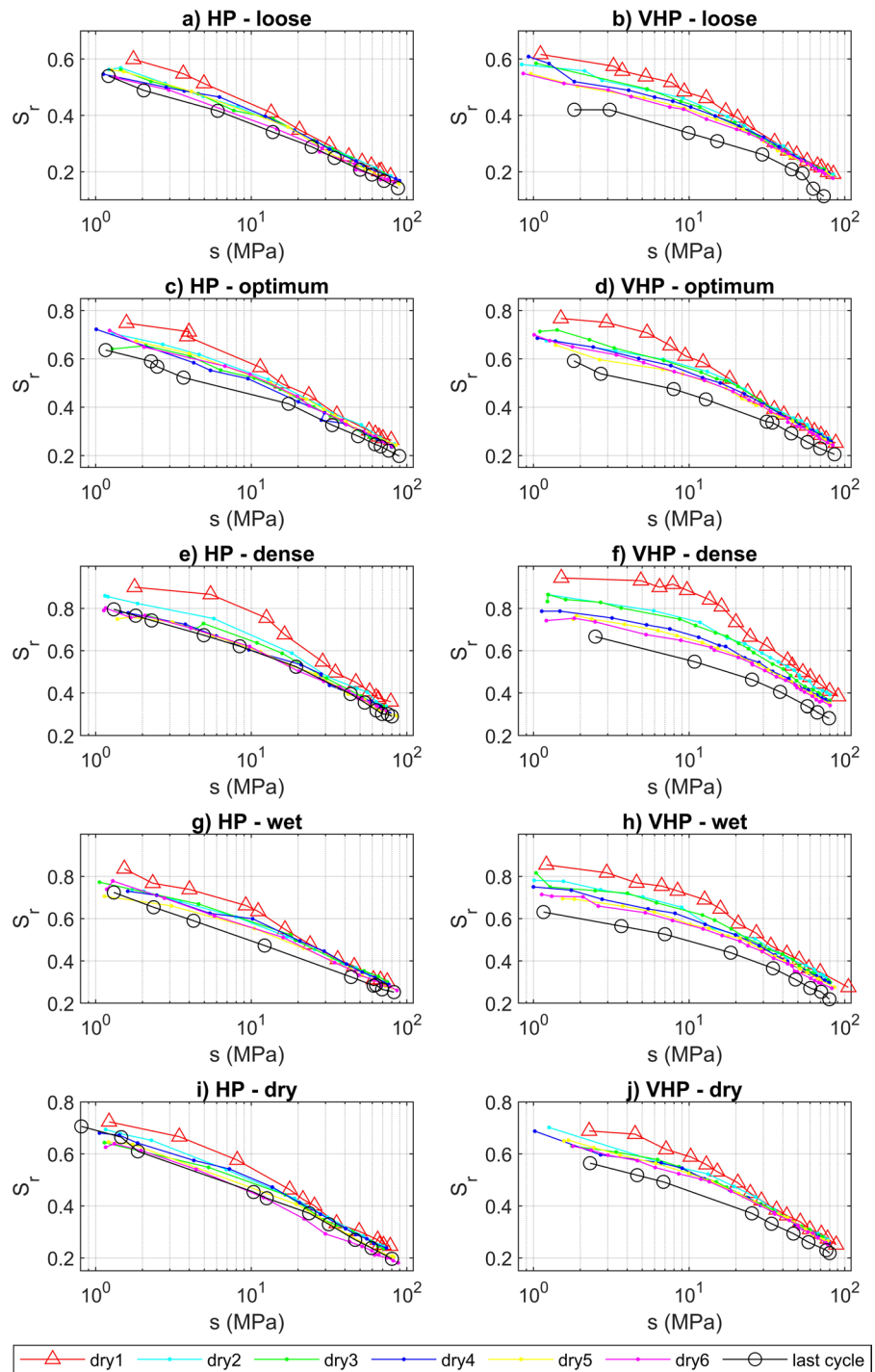


**Fig. 1** Representation of the different compaction conditions and respective compaction curve of each clay plasticity (HP: high plasticity; VHP: very high plasticity)

and the water content of the shrinkage limit (Croney 1977; Dias et al. 2023a, b).

During the drying–wetting cycles, total suction, the weight, and the dimensions of the samples were measured at regular intervals. Each cycle was composed of a drying phase (from 1 to 80 MPa) followed by a wetting phase (from 80 to 1 MPa). During the drying phase, the samples were exposed to the laboratory environment (temperature of  $20 \pm 2$  °C and relative humidity of approximately 50%) for approximately 20 to 30 min and then the samples were sealed for between 30 min and 24 h depending on the

**Fig. 2** Drying soil–water retention curves of high plasticity (HP) and very high plasticity (VHP) clay samples at five different initial compaction conditions

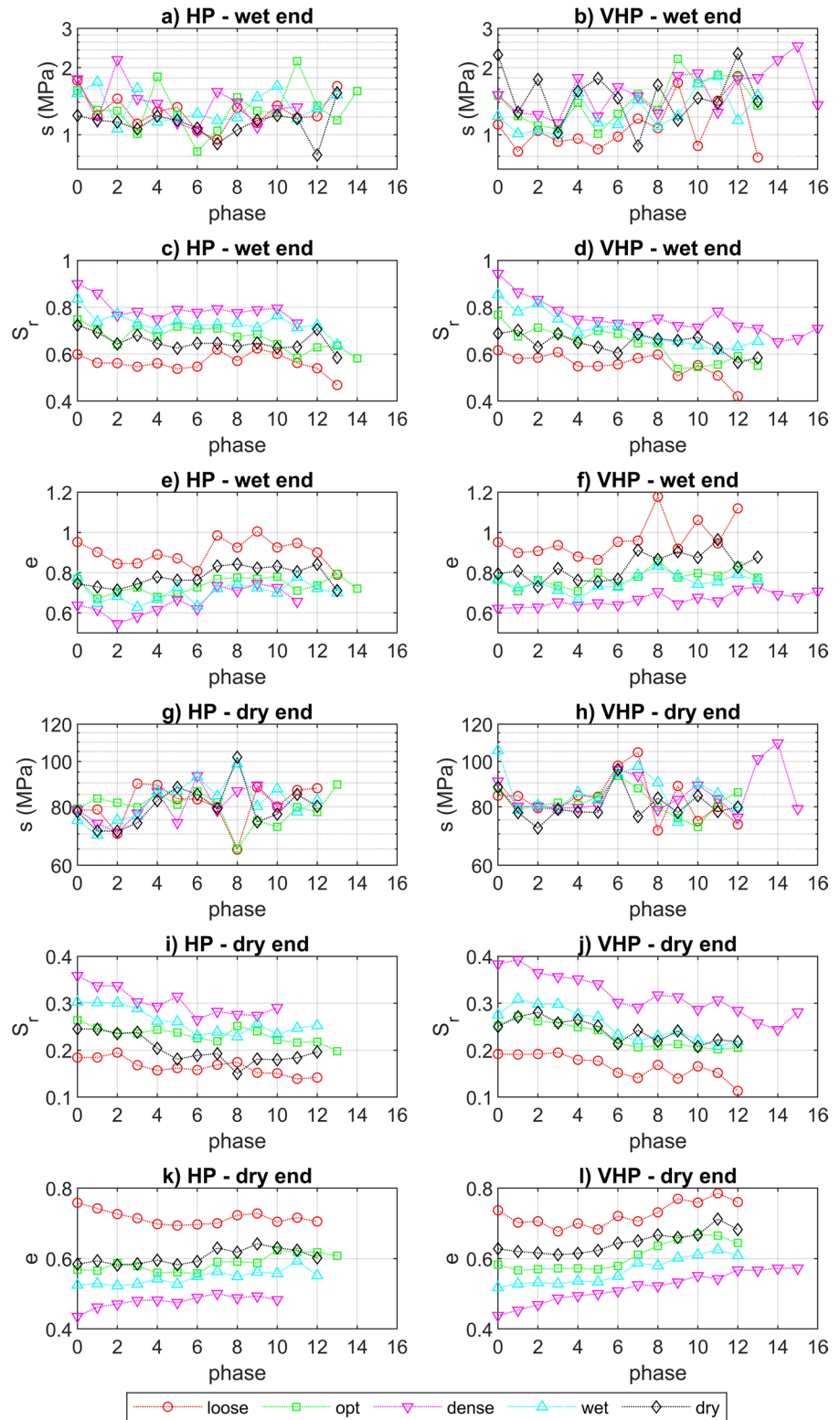


sample’s moisture level to allow the water to redistribute before each measurement.

The wetting phase was accomplished in steps in which 0.01 to 0.02 g of distilled water were added to

the samples with a syringe and the water was allowed to redistribute in a sealed container for a period of 30 min to 24 h depending on the sample’s moisture level, similarly to the drying phase. However, in the

**Fig. 3** Total suction ( $s$ ), degree of saturation ( $S_r$ ) and void ratio ( $e$ ) of high plasticity (HP) and very high plasticity (VHP) clay samples at five different initial compaction conditions at the end of each drying and wetting phase





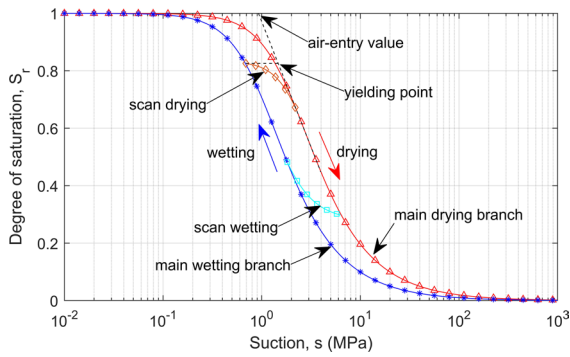


**Fig. 4** Representation of the main loop formed by the ‘main drying’ (triangles) and ‘main wetting’ (stars) branches of the soil–water retention curve (SWRC), and the ‘scan drying’ (diamonds) and ‘scan wetting’ (squares) SWRCs. The air-entry value of the ‘main drying’ SWRC and the yielding point of the ‘scan drying’ curve are identified

present work, the analysis of results focuses only on the drying phases.

After the monitored six cycles had been performed, the samples were subjected to a further variable number of cycles in which only the start and end condition was monitored. The total number of cycles varied between 11 and 16 (Table 2). The last cycle performed on the samples was again monitored with regular measurement of suction, water content and void ratio to obtain the last drying SWRC.

### 3 Soil–Water Retention Curves

#### 3.1 Evolution of Soil–Water Retention Curves

The experimental drying SWRC measurements of the first six cycles (cycle 1 to 6) and the last cycle (after more than ten cycles) represented in Fig. 2 provides an insight into the evolution of hydraulic properties of London Clay considering not only compaction density, but also the fabric, through the comparison of soil samples compacted at different water contents (Dias et al. 2023b). The rigour in this data set can be observed in the replicability of the results for the two plasticity clays. Figure 3 shows the total suction ( $s$ ), degree of saturation ( $S_r$ ) and void ratio ( $e$ ) at the end of each wetting and drying phase, i.e., the conditions at the extremes of each cycle.

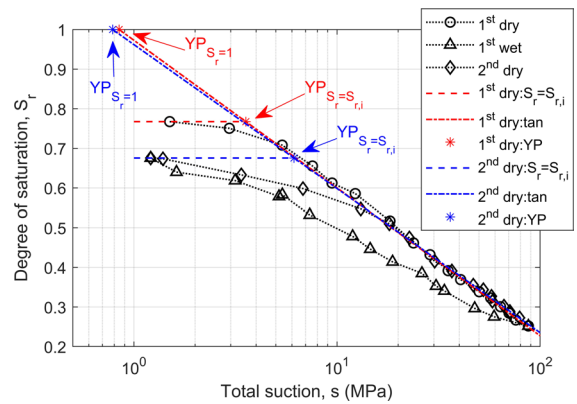


**Fig. 5** Scanning soil–water retention curves (SWRCs) of the sample ‘optimum’ of the very high plasticity clay. Constructions of the bi-linear SWRC model are composed of a horizontal line ( $S_r = S_{r,i}$ ), which intercepts the fitted line to the linear portion of the SWRC (tan) at the yielding point (YP).

The actual suction cycle was performed between  $1.30 \pm 0.27$  MPa and  $81.04 \pm 7.27$  MPa for the HP clay samples and between  $1.40 \pm 0.38$  MPa and  $83.95 \pm 8.20$  MPa for the VHP clay samples (Fig. 3a, b, g, h). It can be seen that the degree of saturation corresponding to the extremes of the cycles decreased with increasing cycles or remained constant (Fig. 3c, d, i, j). The change in the degree of saturation was more evident in the samples with higher degree of saturation at compaction.

The void ratio at the extremes of the cycles presented opposing behaviours depending on the compaction conditions (Fig. 3e, f, k, l). Soil compacted at a lower void ratio (‘dense’ specimens) present a trend of progressive swelling with increasing number of cycles, which could be explained by the formation of cracks upon drying. The ‘loose’ samples show progressive densification, mainly in the first six cycles, after which greater oscillations in the extreme suction values imposed on the samples may have caused an inversion of this behaviour. The remaining samples present an evolution of the void ratio at the extremes of the cycles contained between the response of the ‘dense’ and ‘loose’ samples. Nowamooz and Masrouri (2010) explained that the progressive swelling and shrinkage due to moisture cycles observed in dense and loose samples, respectively, is caused by the rearrangement of the soil structure (fabric).

The drying SWRCs in Fig. 2 show that samples compacted at lower void ratio present SWRCs that start at progressively higher degrees of saturation. For example, Fig. 2a shows a loose sample starting from around  $S_r=0.6$ , the optimum sample (Fig. 2c) starts from  $S_r=0.75$  and the dense sample (Fig. 2e) starts from  $S_r=0.85$ . This can be seen in trends observed in Fig. 3c–f. It might be thought that this trend in the SWRCs of different samples could be represented in the suction-void ratio-degree of saturation space, as proposed by Gallipoli et al. (2003). However, the evolution of the SWRCs with drying–wetting cycles would not fit within this surface because the scanning SWRCs propagate towards lower suctions (Fig. 2), while the void ratio at the end of the drying phase propagates towards lower or higher void ratios depending on the compaction conditions (Fig. 3k, l). Therefore, in the present study it is found that using the initial degree of saturation (that incorporates the volumetric state of the specimen) provides a better representation of the initial state. This evolution of the initial degree of saturation may be caused by the accumulation of volumetric deformations, a change in the fabric due to particle rearrangement, or air-entrapment.

The first drying curve initiated at a higher degree of saturation and water content than any of the remaining phases, even though the initial suction of the first drying phase ‘dry 1’ ranged from 1.11 to 2.28 MPa (Table 2), which was similar to the initial suction of the remaining phases (1 MPa). These observations are in agreement with the conceptual model of Toll (1995), as the first drying phase corresponds to a virgin drying phase and the subsequent cycles correspond to scanning curves that are less steep. Then, the evolution of the scanning curves towards lower suction values and a decrease in the slope, can be observed by comparing the first drying phase (red triangles) to the last drying phase (black circles) in Fig. 4. This observation is consistent with other studies (Lin and Cerato 2013; Stirling et al. 2017; Liu et al. 2020, 2021; Wen et al. 2020).

### 3.2 Analysis of Soil–Water Retention Curves

A conceptual picture of water retention behaviour can be visualised by considering a full cycle of drying and wetting (starting from a zero suction state and continuing to an oven dry condition).

This forms a loop defined by the ‘main drying’ and ‘main wetting’ SWRC, which are different due to hysteresis as illustrated in Fig. 4. Cycles of drying and wetting, in which full drying or complete saturation are not attained, occur within this main loop and are here referred to as ‘scanning curves’, also indicated in Fig. 4. The scanning curves are of interest because, in normal conditions, the soil in the field is likely to follow scanning curves due to the irregular patterns of rainfall and evaporation (Smethurst et al. 2012). Rainfall will cause the soil to wet after a period of drying, but very often without the soil ever reaching full saturation. Similarly, evaporation, after a rainy period, will induce drying but it is unlikely for the soil to ever reach zero water content in the field.

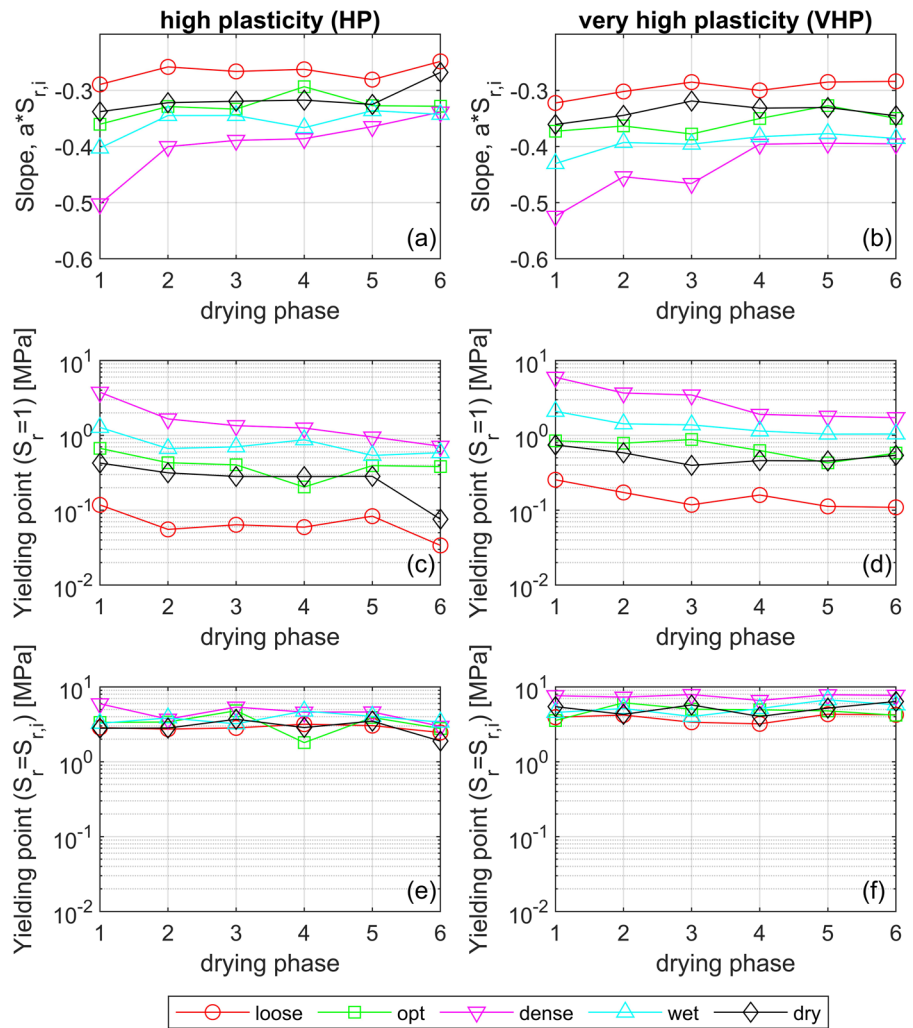
On a SWRC starting from saturation, the air-entry value (AEV) corresponds to the transition between a saturated state and the desaturation curve, when air enters the soil voids (Fig. 4). On the scanning curves, since the soil is already unsaturated, strictly the transition point should not be referred as the AEV (as air has previously entered the soil), thus this transition is here referred as a yield point (YP) that corresponds to the change of the slope of the scanning curve from non-linear to linear. The AEV is the YP correspondent to an initial saturated state.

In this study, the drying–wetting cycles were performed while maintaining the soil samples constantly under unsaturated conditions, and the interpretation of the SWRCs was adapted to take into account the tested suction range (1–80 MPa). Figure 5 shows the first drying, first wetting and second drying phases of a test to illustrate the soil behaviour and analysis of results.

The yield points were identified adopting similar constructions to the ones used to identify the AEV as presented in the schematic curves in Fig. 4. Two different methods of determining the SWRC yield point are here proposed, which are exemplified in Fig. 5 on experimental data. The two interpretations of yielding points are the suction corresponding to the intercept of the tangent to the linear portion of the SWRC with different degrees of saturation ( $S_r$ ): (i)  $S_r = 1$ ; and (ii)  $S_r = S_{r,i}$ , in which  $S_{r,i}$  is the initial degree of saturation of each drying phase. The first method was studied because if the soil does not present a bimodal pore-size distribution, method (i) should provide the real AEV. The second method provides a YP



**Fig. 6** Evolution of the slope of the linear portion of the soil–water retention curve ( $a \cdot S_{r,i}$ ), yield point using method (i) ( $S_r = 1$ ), yield point obtained using method (ii) ( $S_r = S_{r,i}$ ), for samples compacted at different initial conditions of high plasticity (HP) and very high plasticity (VHP) clay



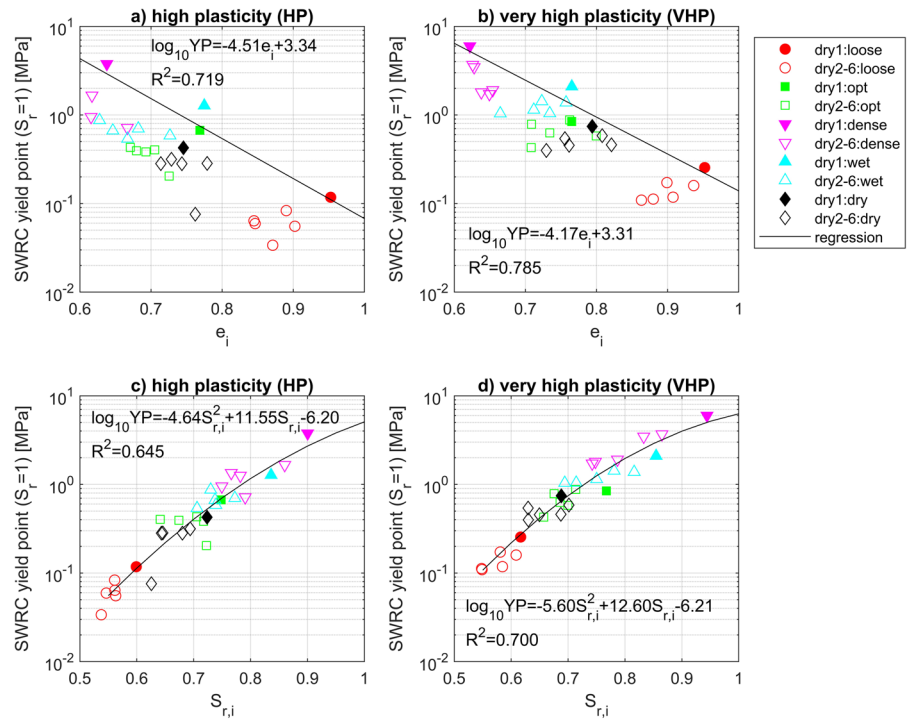
that corresponds to the actual change in the curvature of the measured SWRCs, which is useful for fittings of models, such as the van Genuchten equation (van Genuchten 1980). Method (ii) was based on Parker and Lenhard (1987), who defined scanning paths by scaling the main branches of the SWRC. The proposed methods are equivalent if the sample starts from saturated conditions, as  $S_r = S_{r,i} = 1$ .

In the linear portion of the SWRC (marked as ‘tan’ in the figure), previously referred to as the transition zone of the SWRC, the suction (represented in logarithmic scale) changes proportionally with the degree of saturation ( $S_r$ ). The tangent to the linear portion of the SWRC was determined by fitting Eq. 1 to the experimental data points, where  $a$  and  $b$  are fitting parameters, and  $s$  is the total suction in MPa. The

degree of saturation ( $S_r$ ) was normalized by dividing it by the initial degree of saturation ( $S_{r,i}$ ), so that  $a \cdot S_{r,i}$  is the slope of the tangent, and  $b \cdot S_{r,i}$  is the interception of the line with the y-axis at  $s = 1$  MPa, which represents the position of the tangent in a semi-logarithmic graph (as in Fig. 5). The parameter  $b$  can be given by Eq. 2, where  $YP_{S_r=1}$  is the intercept of the yielding point obtained by method (i), for which the evolution of  $YP_{S_r=1}$  will be discussed instead of parameter  $b$ . The parameters  $a$  and  $b$  were fitted using the least-square method.

$$\frac{S_r}{S_{r,i}} = a \cdot \log s + b \tag{1}$$

**Fig. 7** Relationships between: **a, b** the void ratio at compaction and the yield point (YP) obtained using method (i) ( $S_r = 1$ ); and **c, d** the initial degree of saturation and the same yield point. Regressions and respective coefficient of determination ( $R^2$ ) for high plasticity (HP) clay on the left and very high plasticity (VHP) clay on the right. Regression in **a, b** using only phase ‘dry 1’ (compaction conditions), and regression in **c, d** using all drying phases



$$b = \frac{1}{S_{r,i}} - a \cdot \log YP_{S_r=1} \quad (2)$$

The linear portion of the SWRC was observed to start at different suction values depending on the drying phase and on the plasticity of the clay. It can be seen in Fig. 4 that the linear portion of the first drying phase of the HP clay started at 10 MPa and the subsequent drying phases at 15 MPa, while the first drying phase of the VHP clay started at 15 MPa and the subsequent drying phases at 18 MPa. Therefore, only the data points corresponding to suctions above these thresholds were used for the fitting of parameters  $a$  and  $b$  (Eq. 1).

#### 4 Effect of Compaction Conditions on the Soil–Water Retention Curve

The three essential parameters identified in the previous section for the characterization of the shape of the studied SWRCs were: the initial degree of saturation at the start of each drying phase ( $S_{r,i}$ ); the slope of the linear portion of the SWRC (represented by parameter  $a$ , Eq. 1); and the yielding point obtained using method (i)  $S_r = 1$ . With these key parameters,

an extra yielding point can be identified using method (ii)  $S_r = S_{r,i}$ . Figure 6 presents the evolution over six drying–wetting cycles of the slope of the linear portion of the drying SWRCs ( $a * S_{r,i}$ , see Eq. 1), and the yielding points obtained using method (i)  $S_r = 1$  and method (ii)  $S_r = S_{r,i}$ .

##### 4.1 The Yield Point

The yield point estimated using method (i)  $S_r = 1$  decreases with degree of saturation at compaction and decreases with progressive cycling (Fig. 6c, d). The yield point obtained with method (ii)  $S_r = S_{r,i}$  does not change significantly with increasing number of cycles as the decreasing initial degree of saturation (as seen in Fig. 5c, d) compensates for the changes in the slope of the linear portion of the SWRCs (Fig. 6a, b).

The change in the yield point was observed to depend on the compaction conditions, and hence relationships between them were investigated. Initially the relationship with void ratio was considered. A relationship did exist for the first drying (Fig. 7a, b), but no unique relationship between YP and void ratio existed for all cycles. In comparison, a unique relationship was found between the yield point and the

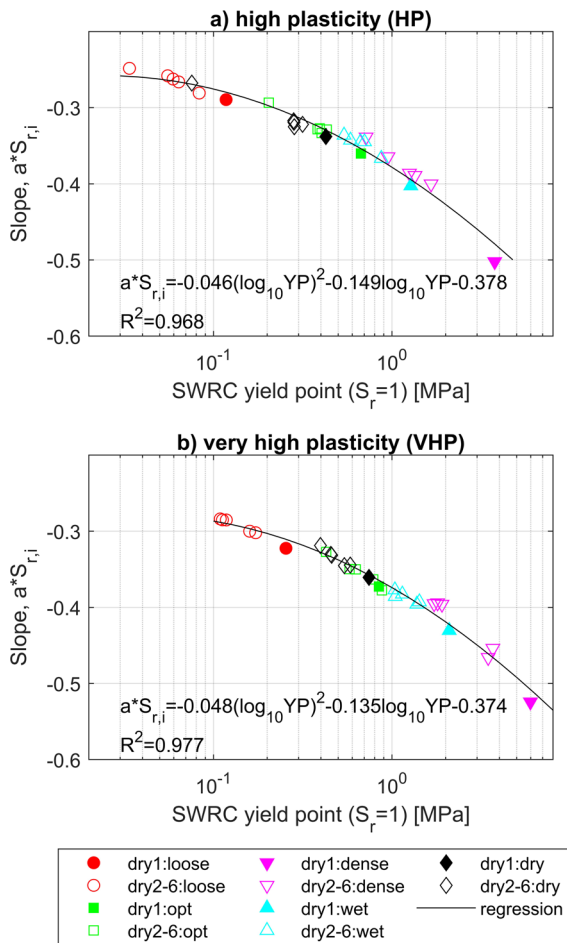


**Fig. 8** Relationship between the slope of the linear portion of the soil–water retention curve ( $a \cdot S_{r,i}$ ) and the yield point (YP) obtained using method (i) ( $S_r = 1$ ). Regression and respective coefficient of determination ( $R^2$ ) for the high plasticity (HP) and very high plasticity (VHP) clay

initial degree of saturation, for which a second-degree polynomial regression line is presented (Fig. 7c, d). The first six cycles were used to produce the relationships, as for these cycles the SWRCs were measured in their entirety whereas later cycles were not. This unique relationship for each soil can therefore be used to predict the shift in YP (method (i)  $S_r = 1$ ).

#### 4.2 The Slope

In Fig. 6a, b, the slope of the linear portion of the SWRCs ( $a \cdot S_{r,i}$ ) is observed to decrease with increasing degree of saturation at compaction and it tends to increase with increasing number of cycles, revealing

fatigue. The first drying phase is the steepest and the slope change becomes less evident with increasing number of cycles, stabilizing after the third drying phase for most samples. However, the slope change did not stabilize over the number of cycles performed for the samples ‘dense’. The greatest increase between the first and last cycle was observed in the dense samples (HP:  $\Delta(a \cdot S_{r,i}) = -0.16$ ; VHP:  $\Delta(a \cdot S_{r,i}) = -0.13$ ) and the remaining samples presented variations ranging from  $-0.03$  to  $-0.07$  for the HP clay and  $-0.02$  to  $-0.04$  for the VHP clay.

It was found that the slope of the linear portion of the SWRC ( $a \cdot S_{r,i}$ ) is related to the yield point (method (i)  $S_r = 1$ ), as shown in Fig. 8, and a relationship was defined through a second-degree polynomial regression for the first six cycles for both the HP and VHP clays. The relationship between the slope of the linear portion of the SWRC and the SWRC yield point shows consistency among samples of different compaction conditions. The slope decreases with increasing yield point, showing that samples compacted at a higher degree of saturation present steeper SWRCs and higher yield points, in agreement with the experimental observations in Fig. 4. The relationship between slope and yield point is also presented with progressive number of cycles (Fig. 8). The first ‘dry1’ phase (filled symbols) and the subsequent cycles (open symbols) show the yield point moving along the curve defined from all results. The SWRCs tend to become less steep with increasing number of cycles following the same trend independently of the compaction conditions. The decrease in the slope is accompanied by a decrease in the yield point. This relationship is very similar for both tested clays, as observed by the similar fitting parameters of the polynomial regression.

### 5 Models for the Estimation of Soil–Water Retention Curves

#### 5.1 Bi-linear Soil–Water Retention Curve Model

The initial degree of saturation, yield point and the slope of the SWRC allow the definition of a bi-linear SWRC model. The bi-linear SWRC model is composed by two sections (dashed lines in Fig. 3): a horizontal line defined by  $S_r = S_{r,i}$ , if  $s \leq YP_{S_r=S_{r,i}}$ ; and the tangent

to the linear portion of the SWRC given by Eq. 1, if  $s > YP_{S_r=S_{r,i}}$  (where  $YP_{S_r=S_{r,i}}$  is the yield point obtained using method (ii)  $S_r = S_{r,i}$ ).

It has been shown that the yield point  $YP_{S_r=1}$  can be estimated from the initial conditions of each drying phase, based on the initial degree of saturation (Fig. 7c, d). The slope of the linear portion of the SWRC, represented by  $a * S_{r,i}$ , can be estimated from  $YP_{S_r=1}$  using the relationships presented in Fig. 8. However, to construct the shape of each scanning curve, we need the yielding point obtained using method (ii)  $YP_{S_r=S_{r,i}}$ . This is given by Eq. 3.

$$\log\left(YP_{S_r=S_{r,i}}\right) = \frac{1-b}{a} \quad (3)$$

In this way, a simple SWRC model can be defined for the estimation of SWRCs based on the initial conditions of the soil independently of the soil compaction conditions. The future evolution of the SWRC with successive cycles can be predicted by knowing the initial degree of saturation and using the relations presented in Figs. 6c, d and 7 to estimate respectively the  $YP_{S_r=1}$  and slope (parameter  $a$ ) necessary to define the bi-linear SWRC model.

## 5.2 Bi-linear to Sigmoidal Soil–Water Retention Curve Model

A more accurate representation of the SWRC can be obtained using the van Genuchten SWRC model (van Genuchten 1980). In the present work, a modified version of this model was adopted as presented in Eq. 4, where  $n$ ,  $m$  and  $c$  are fitting parameters. The parameters  $n$  and  $m$  control the slope of the SWRC. In the present work,  $n$  and  $m$  were not determined by data fitting but from the already determined bi-linear model. The parameters  $n$  and  $m$  were determined by solving the system Eq. 1 = Eq. 4 for two data points: (a) the upper boundary of the linear portion of the SWRC; and (b) the last point of the drying phase. The SWRC predicted by the sigmoidal model is forced to be equal to the bi-linear SWRC in those two points, that were selected to be able to capture the slope of the bi-linear SWRC (i.e. two points on the linear portion above the yield point). Hence, the first point (a) was the suction corresponding to twice the estimated  $YP_{S_r=S_{r,i}}$  (approximately 15 MPa for the HP clay and 18 MPa for the VHP clay) with the respective degree of saturation

estimated by the bi-linear model. The second point (b) was the maximum suction and respective degree of saturation estimated by the bi-linear model. The system Eq. 1 = Eq. 4 was solved using the MATLAB function ‘fsolve’ for a non-linear system of equations.

$$\frac{S_r}{S_{r,i}} = \left[ 1 + \left( \frac{s}{c \cdot YP_{S_r=S_{r,i}}} \right)^n \right]^{-m} \quad (4)$$

The parameter  $c$  was adopted to be equal to 10 in the present work as it was found to be necessary to fix this to help the fitting of the SWRCs. Different values of the parameter  $c$  were tested to maximize the coefficient of determination ( $R^2$ ) for all samples for the first six cycles and a value of 10 was found to give the best fit. In this way, the fitting parameters of the van Genuchten SWRC model can be estimated from the bi-linear model.

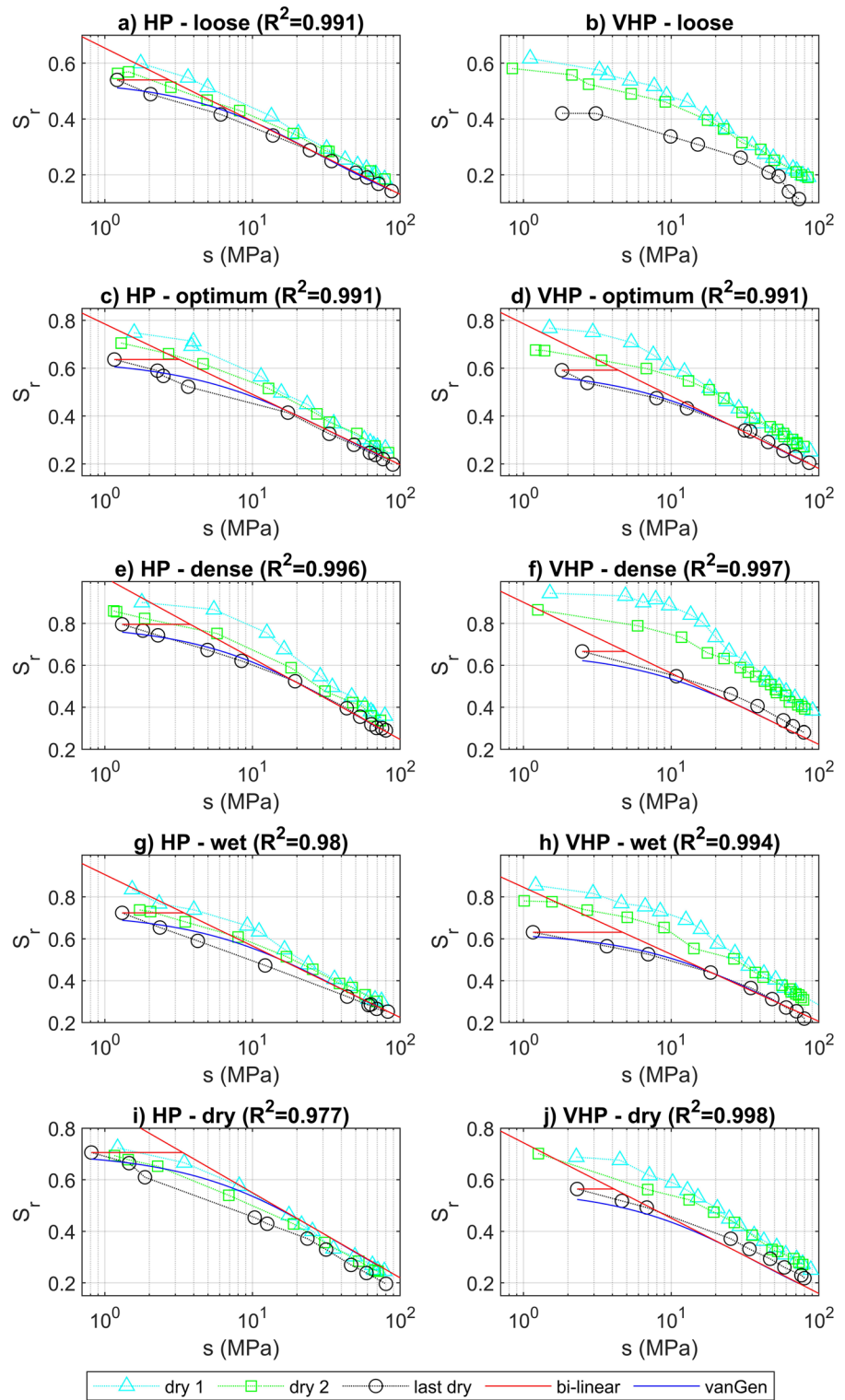
## 6 Prediction of Soil–Water Retention Curves

Figure 9 shows predicted SWRCs using the bi-linear SWRC model and the van Genuchten SWRC model plotted over the experimental measurements of the first, second and last drying SWRC. The models were fitted using the data of the first six drying SWRCs as described above and were then used to predict the drying SWRC of the last cycle, which varied between the 11th and the 16th cycle (Table 2).

The bi-linear SWRC model estimations, represented by red lines in Fig. 9, were able to identify properly the position and slope of the linear portion of the last drying SWRC (black circles). The tangent line (defined by Eq. 1) overlaps the experimental measurements over the linear portion of the SWRC. The bi-linear SWRC estimation produces an upper boundary to the SWRC in the non-linear portion of the SWRC.

The bi-linear model is then used to create the van Genuchten model, shown by dark blue lines in Fig. 9. A good agreement was found between the van Genuchten model estimations and the experimental data as observed by the obtained coefficient of determination ( $R^2$ , reported in Fig. 9) that varied between 0.977 and 0.998. Exceptionally good estimations of the SWRCs were obtained for the sample ‘loose’,

**Fig. 9** Predicted soil–water retention curves (SWRCs) of the last drying phase using the bi-linear and the van Genuchten SWRC models. Comparison with experimental data of the phases ‘dry 1’, ‘dry 2’ and the last drying of samples compacted at different initial conditions of (left) high plasticity and (right) very high plasticity clay, HP and VHP respectively





and ‘dense’ of the HP clay (Fig. 9a, e), and the samples ‘optimum’, and ‘wet’ of the VHP clay (Fig. 9d, h) over the entire range of suctions. However, a good SWRC estimation with the van Genuchten model strongly depends on a good estimation of the tangent to the linear portion of the SWRC and the correct choice of the parameter  $c$ .

The model could not be used in the case of the loose sample of VHP clay (Fig. 9b) because the initial degree of saturation of the last cycle ( $S_{r,i} = 0.42$ ) was out of the range used for the calibration of the relationships in Fig. 7d ( $0.54 \leq S_{r,i} \leq 0.94$ ). It is possible that further to the natural change of SWRC, the handling of the sample during testing led to losses of material and excessive deformations. This sample was more sensitive to accidental deformations and breakage than other samples due to its low density.

## 7 Discussion

The model was validated in the previous section, however, these results could be extended for higher number of cycles. For further increase in the number of drying–wetting cycles, the presented model indicates that the yielding point of the SWRC will continue to decrease, while the slope will tend to stabilize. Nonetheless, the change in the SWRC with increasing number of cycles will depend on the degree of saturation attained upon wetting, i.e., on the initial degree of saturation, taking into account possible changes in void ratio occurring during the wetting process. In this way, if the degree of saturation at the end of wetting periods remains unchanged with increasing number of cycles, then no changes in the subsequent drying SWRCs will be expected.

The presented relationships (Figs. 7, 8) were fitted using six drying SWRCs on five samples compacted at different water content and density. However, the relationships between the degree of saturation and the yield point (Fig. 7c, d), and the yield point and the slope of the linear portion of the SWRC (Fig. 8) could possibly be established using a smaller data set. As observed in the previous sections, these relationships are maintained with progressive drying–wetting cycling independently of the compaction conditions.

Moisture cycles lead to a continuous deterioration of the soil properties, in particular, these cycles lead to changes in the SWRC that result in soil strength

reduction because of suction loss (Stirling et al. 2021). The proposed method will allow engineers and researchers to predict the evolution of the SWRC of a compacted clay without the need for an extensive experimental program. Using the proposed method, the SWRC of clay compacted at any condition and exposed to an unknown number of moisture cycles constrained within a limited range of suction values could be estimated. Predicting this ever-changing property has the potential to equip modellers with the ability to simulate earthworks exposed to climatic changes, accounting for the soil hydro-mechanical properties in the present and future.

## 8 Conclusions

In the present study, soil water retention curves (SWRCs) of compacted samples of high and very high plasticity London clay were investigated over 10–16 cycles of drying and wetting between 1 and 80 MPa. The experimental data obtained showed that SWRCs evolve with increasing number of cycles: the yield point (equivalent to the air-entry value) decreased and the linear portion of the SWRC became less steep. In this way, the suction values became lower with increasing number of moisture cycles for a given degree of saturation.

The change in the SWRCs depends on the soil conditions at the beginning of each drying phase, represented by the initial degree of saturation, and on the plasticity of the clay. A relationship was established between the initial degree of saturation and the yield point of the SWRCs. A relationship between the yield point and the slope of the linear portion of the SWRC was also established. These two relationships can be used to predict the evolution of the SWRC because they are preserved with increasing number of drying–wetting cycles. They form the basis of a model capable of predicting drying SWRCs from any starting condition. The SWRC model was tested by producing estimations of the latest (> 10th) drying phase obtained on the tested samples.

An initial bi-linear model established an upper boundary of the SWRC in which the prediction overlaps the experimental data over the linear portion of the SWRC. Once the bi-linear model was defined, a van Genuchten model, constrained by the initial bi-linear model, was used to predict the SWRC.



Therefore, the presented results show that the drying SWRCs can be predicted based on the soil state (water content and void ratio combined into degree of saturation) at the start of each drying cycle, which can be useful in the modelling of old embankments for which the initial compaction conditions and previous number of wetting and drying cycles are not known. Furthermore, the present model allows the prediction of future changes in the SWRC with changing climatic conditions without the need for further experimental investigation. The findings and method presented in this work should facilitate the modelling of the suction changes in these old embankments, which are most vulnerable to failure in the case of extreme weather events.

**Acknowledgements** The work presented is an output of the ACHILLES programme grant (Programme Grant Number EP/R034575/1) funded by the UK Engineering and Physical Sciences Research Council (EPSRC). The authors would like to acknowledge Stephen Richardson and Kevan Longley at Durham University for their assistance with the laboratory testing. For the purpose of open access, the authors have applied a Creative Commons Attribution (CC BY) licence to any Accepted Manuscript version arising.

**Funding** The work presented is an output of the ACHILLES programme grant (Programme Grant Number EP/R034575/1) funded by the UK Engineering and Physical Sciences Research Council (EPSRC).

**Data Availability** The datasets generated during and/or analysed during the current study are available in the Durham Research Online repository at <https://doi.org/10.15128/r1zc77sq19n>.

## Declarations

**Conflict of interest** The authors have no relevant financial or non-financial interests to disclose.

**Open Access** This article is licensed under a Creative Commons Attribution 4.0 International License, which permits use, sharing, adaptation, distribution and reproduction in any medium or format, as long as you give appropriate credit to the original author(s) and the source, provide a link to the Creative Commons licence, and indicate if changes were made. The images or other third party material in this article are included in the article's Creative Commons licence, unless indicated otherwise in a credit line to the material. If material is not included in the article's Creative Commons licence and your intended use is not permitted by statutory regulation or exceeds the permitted use, you will need to obtain permission directly from the copyright holder. To view a copy of this licence, visit <http://creativecommons.org/licenses/by/4.0/>.

## References

- Al Haj KMA, Standing JR (2016) Soil water retention curves representing two tropical clay soils from Sudan. *Geotechnique* 66(1):71–84. <https://doi.org/10.1680/jgeot.15.P.086>
- Azizi A, Musso G, Jommi C (2020) Effects of repeated hydraulic loads on microstructure and hydraulic behaviour of a compacted clayey silt. *Can Geotech J* 57(1):100–114. <https://doi.org/10.1139/cgj-2018-0505>
- Birle E, Heyer D, Vogt N (2008) Influence of the initial water content and dry density on the soil–water retention curve and the shrinkage behavior of a compacted clay. *Acta Geotech* 3(3):191–200. <https://doi.org/10.1007/s11440-008-0059-y>
- BSI (1990) BS 1377:1990-Methods of test for soils for civil engineering purposes
- Clarke D, Smethurst JA (2010) Effects of climate change on cycles of wetting and drying in engineered clay slopes in England. *Q J Eng Geol Hydrogeol* 43(4):473–486. <https://doi.org/10.1144/1470-9236/08-106>
- Cornelis WM, Corluy J, Medina H, Díaz J, Hartmann R, Van Meirvenne M, Ruiz ME (2006) Measuring and modelling the soil shrinkage characteristic curve. *Geoderma* 137(1–2):179–191. <https://doi.org/10.1016/j.geoderma.2006.08.022>
- Cronley D (1977) The design and performance of road pavements. HMSO, London
- Dias AS, Hughes P, Toll D (2023a) Irreversible effects of drying–wetting cycles on shrinkage and water retention of compacted London clay. *E3S Web Conf* 382:06003. <https://doi.org/10.1051/e3sconf/202338206003>
- Dias AS, Hughes PN, Toll DG, Glendinning S (2023b) A simple method to determine soil–water retention curves of compacted active clays. *Transp Geotech*. <https://doi.org/10.1016/j.trgeo.2023.101138>
- Dif A, Bluemel W (1991) Expansive soils under cyclic drying and wetting. *Geotech Test J* 14(1):96. <https://doi.org/10.1520/GTJ10196J>
- Estabragh AR, Parsaei B, Javadi AA (2015) Laboratory investigation of the effect of cyclic wetting and drying on the behaviour of an expansive soil. *Soils Found* 55(2):304–314. <https://doi.org/10.1016/j.sandf.2015.02.007>
- Ferranti E, Chapman L, Lee S, Jaroszowski D, Lowe C, McCulloch S, Quinn A (2018) The hottest July day on the railway network: insights and thoughts for the future. *Meteorol Appl* 25(2):195–208. <https://doi.org/10.1002/met.1681>
- Fredlund DG (2000) The 1999 R.M. Hardy lecture: the implementation of unsaturated soil mechanics into geotechnical engineering. *Can Geotech J* 37(5):963–986. <https://doi.org/10.1139/t00-026>
- Gallipoli D, Wheeler SJ, Karstunen M (2003) Modelling the variation of degree of saturation in a deformable unsaturated soil. *Geotechnique* 53(1):105–112. <https://doi.org/10.1680/geot.2003.53.1.105>
- Jayanth S, Iyer K, Singh DN (2012) Influence of drying and wetting cycles on SWCCs of fine-grained soils. *J Test Eval* 40(3):104184. <https://doi.org/10.1520/JTE104184>

- Karube D, Kawai K (2001) The role of pore water in the mechanical behavior of unsaturated soils. *Geotech Geol Eng* 19:211–241. <https://doi.org/10.1023/A:1013188200053>
- Kawai K, Kato S, Karube D (2020) The model of water retention curve considering effects of void ratio. *Unsaturated soils for Asia*. CRC Press, pp 329–334
- Leong EC, Wijaya M (2015) Universal soil shrinkage curve equation. *Geoderma* 237:78–87. <https://doi.org/10.1016/j.geoderma.2014.08.012>
- Lin B, Cerato AB (2013) Hysteretic soil water characteristics and cyclic swell–shrink paths of compacted expansive soils. *Bull Eng Geol Environ* 72(1):61–70. <https://doi.org/10.1007/s10064-012-0450-7>
- Liu G, Toll DG, Kong L, Asquith JD (2020) Matric suction and volume characteristics of compacted clay soil under drying and wetting cycles. *Geotech Test J* 43(2):464–479. <https://doi.org/10.1520/GTJ20170310>
- Mishra PN, Zhang Y, Bhuyan MH, Scheuermann A (2020) Anisotropy in volume change behaviour of soils during shrinkage. *Acta Geotech* 15(12):3399–3414. <https://doi.org/10.1007/s11440-020-01015-6>
- Muddle D, Briggs KM, Dashwood C, Dijkstra T (2015) The influence of slope geology on landslide occurrence during extreme rainfall. In: XVI European conference on soil mechanics and geotechnical engineering. Unspecified (C) 2015. IOS Press, UK
- Ng CWW, Peparah-Manu D (2023) Pore structure effects on the water retention behaviour of a compacted silty sand soil subjected to drying–wetting cycles. *Eng Geol* 313(March 2022):106963. <https://doi.org/10.1016/j.enggeo.2022.106963>
- Nowamooz H, Masroufi F (2010) Relationships between soil fabric and suction cycles in compacted swelling soils. *Eng Geol* 114(3–4):444–455. <https://doi.org/10.1016/j.enggeo.2010.06.005>
- Parker JC, Lenhard RJ (1987) A model for hysteretic constitutive relations governing multiphase flow: 1. Saturation–pressure relations. *Water Resour Res* 23(12):2187–2196. <https://doi.org/10.1029/WR023i012p02187>
- Romero E, Gens A, Lloret A (1999) Water permeability, water retention and microstructure of unsaturated compacted boom clay. *Eng Geol* 54(1–2):117–127. [https://doi.org/10.1016/S0013-7952\(99\)00067-8](https://doi.org/10.1016/S0013-7952(99)00067-8)
- Romero E, Vaunat J (2000) Retention curves of deformable clays. In: Proceedings of an international workshop on unsaturated soils, experimental evidence and theoretical approaches in unsaturated soils. pp 91–106
- Romero E, Della VECCHIAG, Jommi C (2011) An insight into the water retention properties of compacted clayey soils. *Géotechnique* 61(4):313–328. <https://doi.org/10.1680/geot.2011.61.4.313>
- Salager S, El Youssoufi MS, Saix C (2010) Definition and experimental determination of a soil–water retention surface. *Can Geotech J* 47(6):609–622. <https://doi.org/10.1139/T09-123>
- Seiphoori A, Ferrari A, Laloui L (2014) Water retention behaviour and microstructural evolution of MX-80 bentonite during wetting and drying cycles. *Géotechnique* 64(9):721–734. <https://doi.org/10.1680/geot.14.P.017>
- Skempton AW (1984) The Colloidal activity of Clays. Selected Papers on Soil Mechanics. Thomassss Telford Publishing, pp 60–64
- Smethurst JA, Clarke D, Powrie W (2012) Factors controlling the seasonal variation in soil water content and pore water pressures within a lightly vegetated clay slope. *Geotechnique* 62(5):429–446. <https://doi.org/10.1680/geot.10.P.097>
- Stirling R, Helm P, Glendinning S, Asquith J, Hughes P, Toll D (2017) Deterioration of geotechnical infrastructure: The influence of asset aging through environmental cycling. In: ICSMGE 2017–19th International Conference on Soil Mechanics and Geotechnical Engineering 2017–Sept, pp. 3199–3202
- Stirling RA, Toll DG, Glendinning S, Helm PR, Yildiz A, Hughes PN, Asquith JD (2021) Weather-driven deterioration processes affecting the performance of embankment slopes. *Géotechnique* 71(11):957–969. <https://doi.org/10.1680/jgeot.19.SiP.038>
- Sun H, Mašín D, Najser J, Neděla V, Navrátilová E (2019) Bentonite microstructure and saturation evolution in wetting–drying cycles evaluated using ESEM, MIP and WRC measurements. *Géotechnique* 69(8):713–726. <https://doi.org/10.1680/jgeot.17.P.253>
- Toll DG (1995) A conceptual model for the drying and wetting of soil. *Proc First Int Conf Unsaturated Soils* 2:805–810
- Tripathy S, Subba Rao KS (2009) Cyclic swell–shrink Behaviour of a compacted expansive soil. *Geotech Geol Eng* 27:89–103. <https://doi.org/10.1007/s10706-008-9214-3>
- van Genuchten MT (1980) A closed-form equation for Predicting the Hydraulic Conductivity of Unsaturated soils. *Soil Sci Soc Am J* 44(5):892–898. <https://doi.org/10.2136/sssaj1980.03615995004400050002x>
- Villar MV (2007) Water retention of two natural compacted bentonites. *Clays Clay Miner* 55(3):311–322. <https://doi.org/10.1346/CCMN.2007.0550307>
- Walker C, Heitor A, Clarke B (2022) Influence of Weather-Driven processes on the performance of UK Transport infrastructure with reference to historic geostructures. *Appl Sci* 12(15):7461. <https://doi.org/10.3390/app12157461>
- Wang HL, Yin ZY, Zhang P, Jin YF (2020) Straightforward prediction for air-entry value of compacted soils using machine learning algorithms. *Eng Geol* 279:105911. <https://doi.org/10.1016/J.ENGGEOL.2020.105911>
- Wen T, Shao L, Guo X, Zhao Y (2020) Experimental investigations of the soil water retention curve under multiple drying–wetting cycles. *Acta Geotech* 15(11):3321–3326. <https://doi.org/10.1007/S11440-020-00964-2/TABLES/4>
- Zeng L, Li F, Liu J, Gao Q, Bian H (2019) Effect of initial gravimetric water content and cyclic wetting–drying on soil–water characteristic curves of disintegrated carbonaceous mudstone. *Transp Saf Environ* 1(3):230–240. <https://doi.org/10.1093/tse/tdz018>

**Publisher's Note** Springer Nature remains neutral with regard to jurisdictional claims in published maps and institutional affiliations.